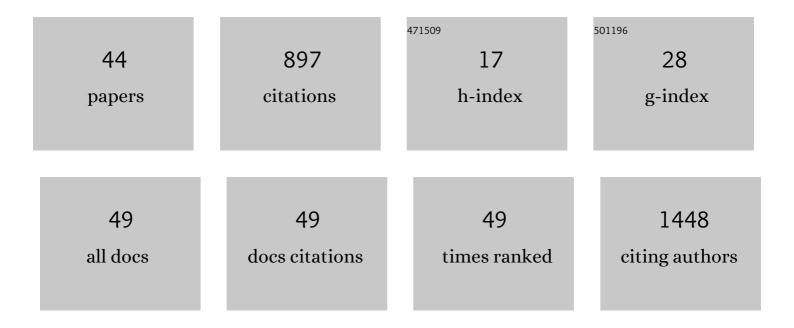
Tamas Varga

List of Publications by Year in descending order

Source: https://exaly.com/author-pdf/5025543/publications.pdf Version: 2024-02-01



TAMAS VADCA

#	Article	IF	CITATIONS
1	Pore-Engineered Metal–Organic Frameworks with Excellent Adsorption of Water and Fluorocarbon Refrigerant for Cooling Applications. Journal of the American Chemical Society, 2017, 139, 10601-10604.	13.7	128
2	Electric field stimulates production of highly conductive microbial OmcZ nanowires. Nature Chemical Biology, 2020, 16, 1136-1142.	8.0	112
3	Unraveling the mysterious failure of Cu/SAPO-34 selective catalytic reduction catalysts. Nature Communications, 2019, 10, 1137.	12.8	99
4	Soil texture and environmental conditions influence the biogeochemical responses of soils to drought and flooding. Communications Earth & Environment, 2021, 2, .	6.8	35
5	Understanding the Electronic Structure Evolution of Epitaxial LaNi _{1–<i>x</i>} Fe _{<i>x</i>} O ₃ Thin Films for Water Oxidation. Nano Letters, 2021, 21, 8324-8331.	9.1	31
6	Soil pore network response to freeze-thaw cycles in permafrost aggregates. Geoderma, 2022, 411, 115674.	5.1	30
7	Strain Accommodation by Facile WO ₆ Octahedral Distortion and Tilting during WO ₃ Heteroepitaxy on SrTiO ₃ (001). ACS Applied Materials & Interfaces, 2014, 6, 14253-14258.	8.0	29
8	Creation and Ordering of Oxygen Vacancies at WO _{3â َ ٱ ٓ} and Perovskite Interfaces. ACS Applied Materials & Interfaces, 2018, 10, 17480-17486.	8.0	29
9	Metal–Organic Framework–Polyacrylonitrile Composite Beads for Xenon Capture. ACS Applied Materials & Interfaces, 2020, 12, 45342-45350.	8.0	25
10	Epitaxial growth of NiTiO3 with a distorted ilmenite structure. Thin Solid Films, 2012, 520, 5534-5541.	1.8	24
11	Inorganic tin aluminophosphate nanocomposite for reductive separation of pertechnetate. Environmental Science: Nano, 2016, 3, 1003-1013.	4.3	24
12	RedOx-controlled sorption of iodine anions by hydrotalcite composites. RSC Advances, 2016, 6, 76042-76055.	3.6	23
13	Insights into the physical and chemical properties of a cement-polymer composite developed for geothermal wellbore applications. Cement and Concrete Composites, 2019, 97, 279-287.	10.7	22
14	Phase transformation kinetics in rolled U-10Âwt. % Mo foil: Effect of post-rolling heat treatment and prior γ-UMo grain size. Journal of Nuclear Materials, 2017, 496, 215-226.	2.7	20
15	Immobilizing Pertechnetate in Ettringite via Sulfate Substitution. Environmental Science & Technology, 2020, 54, 13610-13618.	10.0	20
16	Coupled Lattice Polarization and Ferromagnetism in Multiferroic NiTiO ₃ Thin Films. ACS Applied Materials & Interfaces, 2017, 9, 21879-21890.	8.0	18
17	Coexistence of weak ferromagnetism and polar lattice distortion in epitaxial NiTiO3 thin films of the LiNbO3-type structure. Journal of Vacuum Science and Technology B:Nanotechnology and Microelectronics, 2013, 31, 030603.	1.2	17
18	The Ability of Soil Pore Network Metrics to Predict Redox Dynamics is Scale Dependent. Soil Systems, 2018, 2, 66.	2.6	16

TAMAS VARGA

#	Article	IF	CITATIONS
19	Chromate Effect on lodate Incorporation into Calcite. ACS Earth and Space Chemistry, 2019, 3, 1624-1630.	2.7	16
20	Tuning piezoelectric properties through epitaxy of La2Ti2O7 and related thin films. Scientific Reports, 2018, 8, 3037.	3.3	15
21	In situ characterization of foam morphology during melting of simulated waste glass using x-ray computed tomography. Ceramics International, 2020, 46, 17176-17185.	4.8	15
22	Calcareous organic matter coatings sequester siderophores in alkaline soils. Science of the Total Environment, 2020, 724, 138250.	8.0	14
23	Preâ€Viking Swedish hillfort glass: A prospective longâ€ŧerm alteration analogue for vitrified nuclear waste. International Journal of Applied Glass Science, 2018, 9, 540-554.	2.0	13
24	What can we learn from in-soil imaging of a live plant: X-ray Computed Tomography and 3D numerical simulation of root-soil system. Rhizosphere, 2017, 3, 259-262.	3.0	12
25	Molecular and Microscopic Insights into the Formation of Soil Organic Matter in a Red Pine Rhizosphere. Soils, 2017, 1, 4.	1.0	12
26	Through a glass darkly: In-situ x-ray computed tomography imaging of feed melting in continuously fed laboratory-scale glass melter. Ceramics International, 2021, 47, 15807-15818.	4.8	11
27	Competitive TcO4–, IO3–, and CrO42– Incorporation into Ettringite. Environmental Science & Technology, 2021, 55, 1057-1066.	10.0	11
28	Polymer-cement composites with adhesion and re-adhesion (healing) to casing capability for geothermal wellbore applications. Cement and Concrete Composites, 2020, 107, 103490.	10.7	9
29	Strain-Dependence of the Structure and Ferroic Properties of Epitaxial NiTiO ₃ Thin Films Grown on Different Substrates. Advances in Condensed Matter Physics, 2015, 2015, 1-9.	1.1	7
30	Strain-dependence of the structure and ferroic properties of epitaxial Ni1â^'xTi1â^'yO3 thin films grown on sapphire substrates. Thin Solid Films, 2015, 578, 113-123.	1.8	7
31	Spatial access and resource limitations control carbon mineralization in soils. Soil Biology and Biochemistry, 2021, 162, 108427.	8.8	7
32	Behavior of iodate substituted ettringite during aqueous leaching. Applied Geochemistry, 2021, 125, 104863.	3.0	6
33	In-situ X-ray and visual observation of foam morphology and behavior at the batch-melt interface during melting of simulated waste glass. Ceramics International, 2022, 48, 7975-7985.	4.8	6
34	Tuning the Charge and Hydrophobicity of Graphene Oxide Membranes by Functionalization with Ionic Liquids at Epoxide Sites. ACS Applied Materials & Interfaces, 2022, 14, 19031-19042.	8.0	6
35	Microstructural evolution and precipitation in \hat{I}^3 -LiAlO2 during ion irradiation. Journal of Applied Physics, 2022, 131, .	2.5	6
36	Inorganic Ba–Sn nanocomposite materials for sulfate sequestration from complex aqueous solutions. Environmental Science: Nano, 2018, 5, 890-903.	4.3	5

TAMAS VARGA

#	Article	IF	CITATIONS
37	Controlling the structure and ferroic properties of strained epitaxial NiTiO3 thin films on sapphire by post-deposition annealing. Thin Solid Films, 2018, 662, 47-53.	1.8	3
38	Evolution of metastable phases during Mg metal corrosion: An <i>in situ</i> cryogenic x-ray photoelectron spectroscopy study. Journal of Vacuum Science and Technology A: Vacuum, Surfaces and Films, 2021, 39, .	2.1	3
39	Extracting Metrics for Three-dimensional Root Systems: Volume and Surface Analysis from In-soil X-ray Computed Tomography Data. Journal of Visualized Experiments, 2016, , .	0.3	2
40	The behavior of iodine in stabilized granular activated carbon and silver mordenite in cementitious waste forms. Journal of Environmental Radioactivity, 2022, 244-245, 106824.	1.7	2
41	An electrochemical technique for controlled dissolution of zirconium based components of light water reactors. RSC Advances, 2019, 9, 1869-1881.	3.6	1
42	Probing the Radial Chemistry of Getter Components in Light Water Reactors via Controlled Electrochemical Dissolution. ACS Omega, 2020, 5, 13578-13587.	3.5	1
43	Ripples at edges of blooming lilies and torn plastic sheets. Biophysical Journal, 2022, 121, 2389-2397.	0.5	1
44	Effects of Microbial-Mineral Interactions on Organic Carbon Stabilization in a Ponderosa Pine Root Zone: A Micro-Scale Approach. Frontiers in Earth Science, 2022, 10, .	1.8	1